Simulating selected magnetic properties of TbxPr1−xAl2, a magnetocaloric compound

Julio C G Tedesco, Vagner Jandre, Alexandre Magnus G Carvalho, Winfried Kockelmann, Daniel M Többens, Lisandro P Cardoso, Adelino A Coelho and Heloisa N Bordallo

Published version information

Citation: Julio C G Tedesco et al 2024 J. Phys.: Condens. Matter 36 145802

DOI: 10.1088/1361-648X/ad19a2

Simulating Selected Magnetic Properties of TbxPr1-xAl2, a Magnetocaloric Compound

IOP Publishing Journal of Physics: Condensed Matter
J. Phys.: Condens. MatterJournal **XX** (XXXX) XXXXXX https://doi.org/XXXX/XXXX

Simulating Selected Magnetic Properties of $Tb_xPr_{1-x}Al_2$, a Magnetocaloric Compound

Julio C. G. Tedesco[1,2,3], Vagner Jandre[1], Alexandre Magnus G. Carvalho[4,5,6], Winfried Kockelmann[7], Daniel M. Többens[8], Lisandro P. Cardoso (currently retired)[3], Adelino A. Coelho (currently retired)[3] and Heloisa N. Bordallo[2]

[1] Polytechnic Institute of the State University of Rio de Janeiro - UERJ
28625-570, Rua Bonfim 25, Vila Amélia, Nova Friburgo, RJ, Brazil

[2] Niels Bohr Institute, University of Copenhagen
2100, Copenhagen, Denmark

[3] Institute of Physics "Gleb Wataghin", Estate University of Campinas – UNICAMP
13083- 859, Campinas, SP, Brazil

[4] Chemical Engineering Department, São Paulo Federal University, 09913-030, Diadema, SP, Brazil

[5] Mechanical Engineering Department, Maringá State University, 87020-900, Maringá, PR, Brazil

[6] Institute of Physics Armando Dias Tavares, State University of Rio de Janeiro – UERJ, 20550-013, Rua São Francisco Xavier, 524, Rio de Janeiro, RJ, Brazil

[7] Science and Technology Facilities Council (STFC), Rutherford Appleton Laboratory, ISIS Facility,
Harwell, OX11 0Qx, United Kingdom

[8] Helmholtz-Zentrum Berlin für Materialien und Energie GmbH (HZB)
Hahn-Meitner-Platz 1, 14109 Berlin, Germany

E-mail: tedesco.jcg@gmail.com
Received xxxxxx
Accepted for publication xxxxxx
Published xxxxxx

Abstract

$Tb_xPr_{1-x}Al_2$ are ferrimagnetic materials exhibiting magnetocaloric effect that have gained considerable attention due to their potential use as an alternative in refrigeration, magnetic sensors and in information storage technology. Here using the mean field approach numerical simulations were conducted for x=0.1, 0.2, 0.3, 0.4, 0.5, and 0.75, to analyse selected physical properties, such as X-ray and neutron powder diffraction, magnetization and heat capacity. The simulations successfully reproduced the experimental data providing a comprehensive characterization and improved understanding of this family of compound.

Keywords: Ferrimagnetism, Rare Earth Intermetallic, Inelastic Neutron Scattering, X-rays and Neutron Powder Diffraction, Magnetocaloric effect.

IOP Publishing Journal of Physics: Condensed Matter
J. Phys.: Condens. MatterJournal **XX** (XXXX) XXXXXX https://doi.org/XXXX/XXXX

1. Introduction

Magnetic substances have always stimulated human curiosity, and regarding current technologies an increased interest in the so-called magnetocaloric effect (MCE) [1–5] has occurred in the recent years [6]. When compared to classic refrigerators, such systems show greater efficiency, reduced CO_2 production, energy savings, and a non-volatile solid refrigerant that can replace greenhouse gas refrigerants [7–9]. Furthermore, these compounds show great potential for usage as information storage technology devices, magnetic random access memory, and magnetic field sensors [10–16] and have been suggested as one of the methods of treating malignant tumors [8]. Therefore, the quest for novel materials exhibiting MCE is extremely important for further developments, making it essential to determine and map the physical properties of possible candidate materials, mainly those related to magnetic refrigeration.

Under these lines, in this study, we examine the relevant physical properties of the series of pseudo-binary compounds $Tb_xPr_{1-x}Al_2$, for $x = 0.10, 0.20, 0.30, 0.40, 0.50$ and 0.75, which exhibits magnetic transition at low temperatures and is thus an interesting alternative in cryocooling magnetocaloric applications [7,15,17]. To provide the mapping of the crystal field and mean field behavior parameters in $Tb_xPr_{1-x}Al_2$, and consequently develop new tools for the analyses of the experimental heat capacity and magnetization curves both as a function of temperature and concentration, we employed a mean field self-consistent approach and crystal field theory to simulate the experimental data.

$Tb_xPr_{1-x}Al_2$ belongs to the $(R1,R2)Al_2$ family, where R1 and R2 are rare earth ions, and their interesting characteristics are related to the different magnetic arrangements that occur due to the coupling between the ions. Ferromagnetism (FM) is observed if the R1 and R2 ions are either light or heavy rare earths. If one of them is light and the other is a heavy rare earth the coupling is antiferromagnetic (AF). Since praseodymium is a light rare earth while terbium is a heavy one, each rare earth in $Tb_xPr_{1-x}Al_2$ family of compounds forms sublattices that couple antiferromagnetically. As each sublattice shows a different behavior as a function of temperature, remarkable features, such as the inverse MCE [18–21] are observed. For example, around $x = 0.26$ the magnetic sublattices tend to compensate each other and for a certain temperature the net magnetization is zero [22]. In $Tb_xPr_{1-x}Al_2$ family of compounds, this temperature is around 25 K. Besides an inverse MCE, exchange bias (EB) -like effect, where a displacement of the magnetic hysteresis cycle occurs, is observed in $Tb_{0.25}Pr_{0.75}Al_2$ and in $Tb_{0.30}Pr_{0.70}Al_2$ [22]. Such behavior is also observed in $Gd_{0.25}Pr_{0.75}Al_2$ [23] and $Ho_{0.25}Nd_{0.75}Al_2$ [24].

The aim of this study is to theoretically described magnetization, specific heat, and neutron diffraction data characterizing the $Tb_xPr_{(1-x)}Al_2$ family of compounds. This approach is crucial for making informed decisions when conducting computational numerical modeling. Some of the properties and characteristics obtained and observed were found to be linearly dependent on ionic concentration, indicating that there is also linearity in the parameters of the model chosen for this study. Here we were able to demonstrate that the structural and magnetic properties of the $Tb_xPr_{(1-x)}Al_2$ compounds can be interpreted using molecular field approximation, where the results obtained describe the behavior of the crystalline field and mean field parameters for the entire phase diagram.

2. Materials and Methods

Bulk samples of the $Tb_xPr_{1-x}Al_2$ compounds were obtained using an arc-melting furnace under argon atmosphere with pure elements with a purity grade of 99.99 and 99.9 wt% for aluminum and rare earths, respectively, as start materials. After the melting process, the samples were thermally treated under an argon atmosphere at 1273 K for 5 hours, resulting in homogeneous samples with weight losses of less than 3%. To conduct the measurements, powder samples were produced by manually grinding the samples to a grain size of approximately 20 μm.

Magnetization (M) and heat capacity (Cp) data as a function of temperature were obtained using a PPMS device from Quantum Design Ltd. $Cp\ versus\ T$ was collected with no applied magnetic field, while a field of 200 Oe was used during the magnetization measurements.

X-ray powder diffraction (XRPD) data was performed using a Philips PW3719 diffractometer with Bragg-Brentano geometry using CuKα radiation, with steps of 0.02° and 5 seconds per point. Neutron powder diffraction (NPD) data were obtained for several temperatures between 2 K and 300 K. Samples with $x = 0.20$ and $x = 0.40$ were measured using a polychromatic beam with neutron wavelengths between 0.2 and 3.5 Å on the GEM time-of-flight neutron diffractometer at ISIS [25], while for $x = 0.30$ data were collected using a wavelength of 1.798 Å on the high-resolution neutron powder diffractometer E9 at the Helmholtz-Zentrum Berlin (HZB, Germany) [26]. The NPD data was analyzed by the Rietveld method using the FULLPROF suite of programs [27]. Data analysis and simulations were performed using the MATHEMATICA software from Wolfram Research, Inc.

IOP Publishing Journal of Physics: Condensed Matter
J. Phys.: Condens. MatterJournal **XX** (XXXX) XXXXXX https://doi.org/XXXX/XXXX

3. Results and Discussions

3.1 X-Ray Powder Diffraction and Magnetization Measurements

The crystal structure of the prepared powder samples was confirmed using XRPD. As for other (rare earth)Al_2 compounds, $Tb_xPr_{1-x}Al_2$ intermetallic crystallizes in the C15 cubic Laves phase structure (Cu_2Mg), with space group $Fd\bar{3}m$ [28]. In this structure, the two different sized tetrahedral cavities formed by equivalent sites of cubic point symmetry Td are occupied by rare earth ions. Aluminum ions, on the other hand, occupy sites at tetrahedral cavities [29–31]. The Al ions occupy $16c$ Wyckoff positions while rare earth ions occupy $8b$ Wyckoff positions. The lattice parameter, a, was obtained using the Rietveld method with the FullProf package, and a linear trend in the function of concentration x was observed. The refinements provide the statistical parameters $GoF < 2.5$ and $R_{WP} < 15\%$. The results for the lattice parameter a *versus* x can also be seen in Figure 1, and are summarized in Table 1.

Field cooling (FC) magnetization *versus* temperature curves for $Tb_xPr_{1-x}Al_2$ with $x = 0.20$, 0.40, 0.50 and 0.75 acquired using a field of $\mu_0 H = 0.02\,T$ can be observed in Figure 2. In this Figure, it is also included the data from $x =$ 0 [32], 0.10 [3], 0.25 [3,22], 0.30 [22], and 1.00 [32] to provide a more general overview. In our FC protocol, the magnetic field was applied in the paramagnetic region and data were collected on cooling. The magnetic temperature transition, T_C, was determined by deriving $M(T)$ curves. One can note the linear tendency of T_C as a function of Tb-concentration resembles other properties of similar compounds in Figure 1.

Table 1. Lattice parameter, a, obtained from Rietveld analysis of the XRPD data together with the magnetic transition temperature T_C, for $Tb_xPr_{1-x}Al_2$.

x	$a\ (\pm 0.001$ Å$)$	$T_C\ (\pm 1$ K$)$	Note
0.00	8.034	32	Ref. [32]
0.10	8.016	36	Ref. [3]
0.20	8.002	44	This work
0.25	7.992	48	Ref. [3]
0.30	7.986	52	Ref. [22]
0.40	7.969	61	This work
0.50	7.950	71	This work
0.75	7.908	90	This work
1.00	7.865	108	Ref. [32]

From these data, except for $x = 0.10$ which has lower magnetic moments than $x = 0.00$, ferrimagnetic behavior was clearly observed. This occurs because at lower temperatures the competition between the two sublattices, framed by Tb and Pr, induces a decrease in the magnetization values. This competition is stronger for concentrations around $x = 0.26$, where the lowest total net magnetization is observed. Furthermore, for $x = 0.20$ and 0.25 anisotropy is also detected and, consequently, negative magnetization occurs, even under applied magnetic fields. As the two sublattices present different temperature behaviors, a compensation temperature, T_{comp}, is induced, thus while at $T = T_{comp}$ the net magnetization cancels, for $T < T_{comp}$ the magnetization is negative.

Despite the presence of a compensation temperature in these compounds, this negative magnetization behavior only manifests at low magnetic fields. While its precise origin remains unclear, it can be inferred that the different magnetic sublattices Tb and Pr induce uniaxial anisotropy [24,33],. Notably, this unidirectional anisotropy is enhanced when a magnetic field is applied during sample cooling, analogous to the phenomenon observed in FM-AFM thin film systems. Like these thin films, an exchange bias-like effect can be observed in cases where the competition between subnetworks is stronger. For samples with a Tb concentration approaching $x = 0.26$, the sublattices yield the lowest ferrimagnetic component. Thus, the conduction electrons introduce a ferromagnetic component, and displacement of the magnetic hysteresis curves, characterizing the EB-like effect. This mechanism is xdiscussed at length in reference [22].

IOP Publishing Journal of Physics: Condensed Matter
J. Phys.: Condens. MatterJournal **XX** (XXXX) XXXXXX https://doi.org/XXXX/XXXX

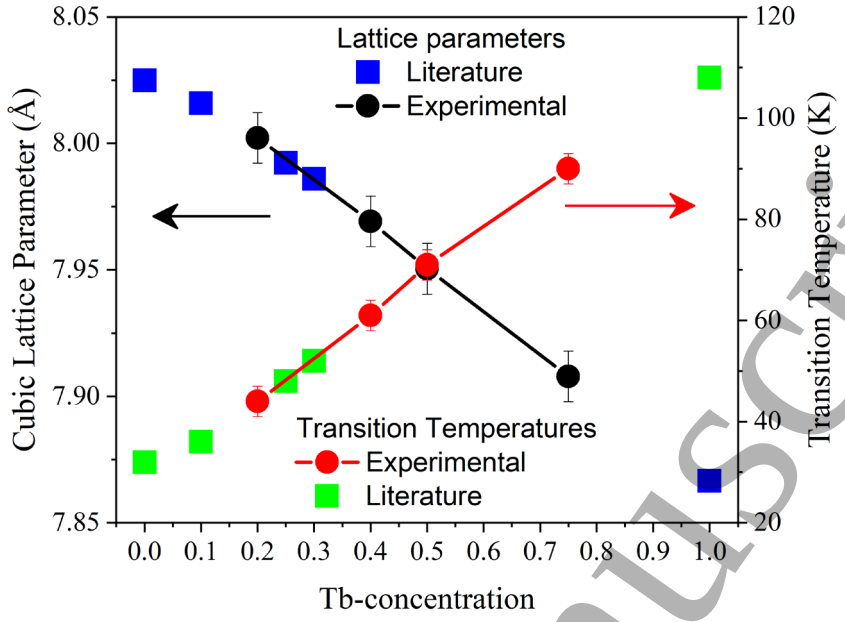

Figure 1. The lattice parameter, a, as a function of Tb-concentration, x, obtained from XRPD patterns refinements – left y-axis – for $Tb_xPr_{1-x}Al_2$. Magnetic transition temperature, T_C, as a function of x – right y-axis – obtained from the FC magnetization data. Circles + Line represent data obtained for this work and squares are the values from literature: $x = 0.00$ and $x = 1.00$ [32]; $x = 0.10$ [3]; 0.25 and 0.30 [22].

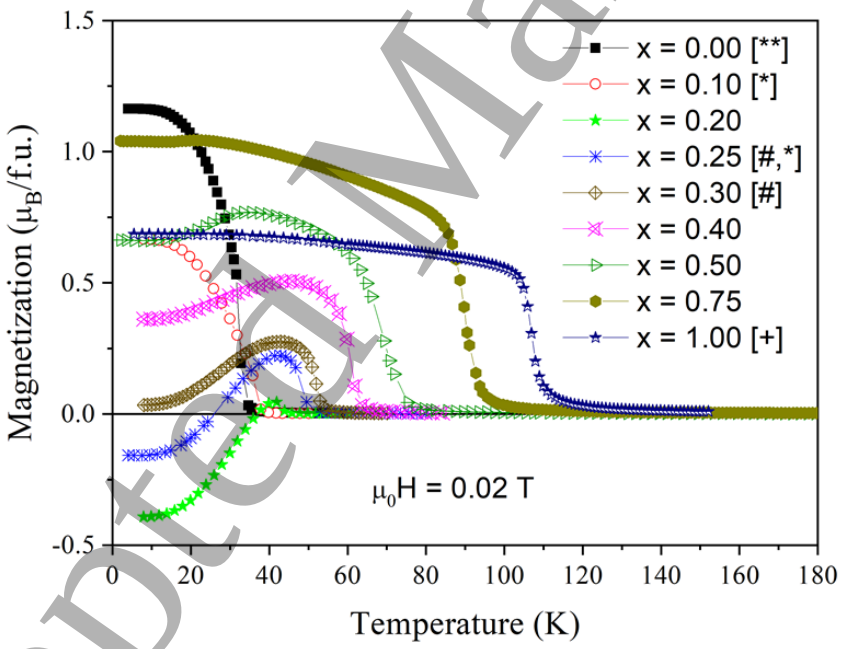

Figure 2. Magnetization data as a function of temperature of $Tb_xPr_{1-x}Al_2$. The protocol used for these measurements is called field cooling (FC), $\mu_0 H = 0.02\ T$. Data for $PrAl_2$ [**],$TbAl_2$ [+], $Tb_{0.25}Pr_{0.75}Al_2$ [#,*], $Tb_{0.30}Pr_{0.70}Al_2$ [#], and $Tb_{0.1}Pr_{0.9}Al_2$ [*] have been previously reported [10, 19, 20].

3.2 Neutron Powder Diffraction

Rietveld refinement of the NPD patterns for $Tb_xPr_{1-x}Al_2$ with $x = 0.20$, $x = 0.30$, and $x = 0.40$ at temperatures between 5 K and 300 K was performed using the FullProf suite of programs [27]. Considering the similarities between these pseudobinary systems and $PrAl_2$, the Pr-Tb coupling was assumed to take place in the $\langle 001 \rangle$ direction, making the c-axis the easy direction. By using this approach, the magnetic and nuclear scattering contributions were refined simultaneously. Figure

IOP Publishing Journal of Physics: Condensed Matter
J. Phys.: Condens. MatterJournal **XX** (XXXX) XXXXXX https://doi.org/XXXX/XXXX

3(a) shows the diffractogram of $Tb_{0.30}Pr_{0.70}Al_2$ acquired at $T = 5\ K$ together with the fitted data.

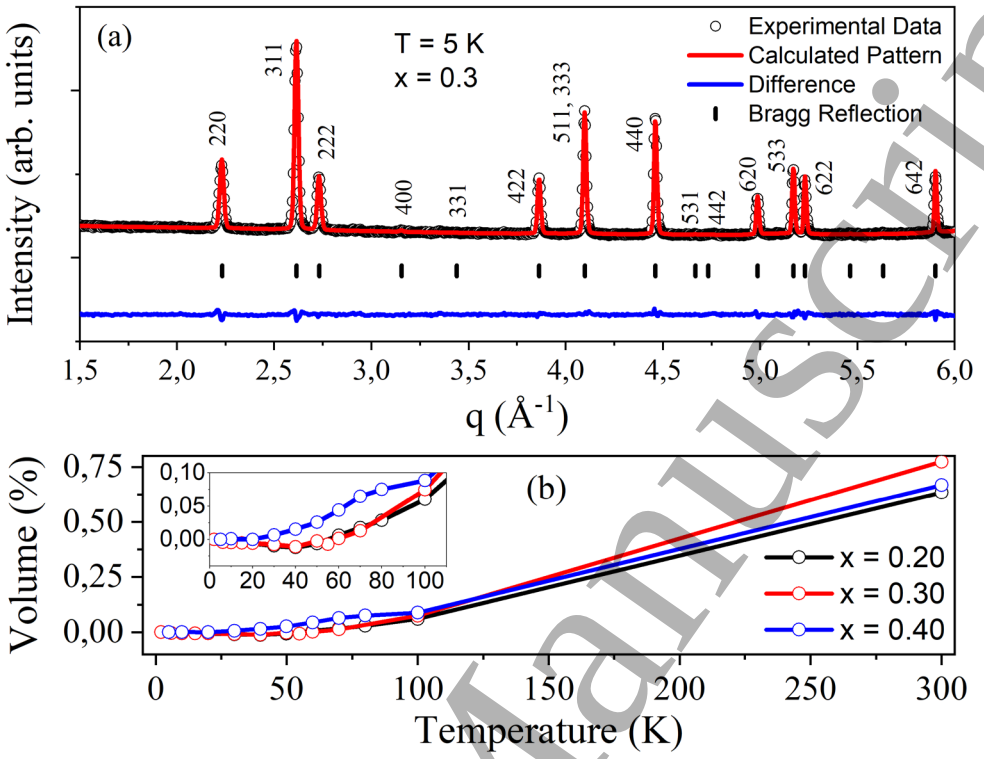

Figure 3. (a) NPD data pattern and respective Rietveld refinement for $Tb_{0.3}Pr_{0.7}Al_2$ collected at $T = 5\ K$ using the E9 diffractometer at HZB with 1.798 Å. The black circles represent the experimental data, while the blue and red lines correspond to the refined intensities and the difference plot between the calculated and observed intensities. The black row of vertical marks shows the calculated positions of the Bragg reflections. (b) Variation of the unit cell volume as a function of temperature.

Table 2. Lattice parameters of $Tb_xPr_{1-x}Al_2$ ($x = 0.20$, 0.30 and 0.40) obtained by Rietveld refinement of NPD data collected using the E9 diffractometer at HZB with 1.798 Å at several temperatures.

Temperature ($\pm 1\ K$)	$a\ (\pm 0.0002$ Å)		
	$x = 0.20$	$x = 0.30$	$x = 0.40$
300	8.0035	7.9859	7.9691
100	7.9883	7.9674	7.9538
80	7.9875	---	7.9538
70	7.9872	7.9658	7.9535
60	7.9869	7.9655	7.9527
55	---	7.9653	---
50	7.9865	7.9654	7.9522
40	7.9864	7.9651	7.9519
30	7.9864	7.9653	7.9517
20	7.9865	7.9653	7.9514
10	7.9867	7.9653	7.9516
5	7.9867	7.9652	7.9515

As expected, because of the almost zero net magnetization without applied field, the $x = 0.30$ sample showed a very small magnetic component. Consequently, Rietveld analysis was performed using the crystal structure only. However, it is worth mentioning that the calculated positions of the magnetic reflections matched the Bragg reflections, i.e., the propagation vector is k = [000]. In all calculations, the refinement parameters χ^2 and R_{WP} were below 10% and 15%, respectively. The lattice parameters obtained by the Rietveld method are shown in Table 2.

The percent variation of the lattice volume as a function of temperature, $(V - V_0)/V_0$, for $x = 0.20$, 0.30 and 0.40

IOP Publishing Journal of Physics: Condensed Matter
J. Phys.: Condens. MatterJournal **XX** (XXXX) XXXXXX https://doi.org/XXXX/XXXX

compounds was also calculated assuming V_0 as the initial volume at 5 K, is shown in Figure 3(b). A very small negative thermal expansion (NTE) for $x = 0.20$ and 0.30 is observed around 50 K (see inset), which was similar to the reported values for $x = 0.10$ and 0.25 [3].

For $x = 0.40$, the lattice parameter increased above $T = 20\ K$. Interestingly, even though the samples with $x = 0.20$ and 0.40 showed low magnetic moments at low temperatures, the magnetic structure had to be considered for all temperatures. However, in these samples, the reflections were only stronger for the first three Bragg reflections, 111, 220, and 311. This behavior was previously observed for $x = 0.10$ and 0.25 [3]. Figure 4 shows the patterns for $Tb_{0.4}Pr_{0.8}Al_2$ obtained at $T = 10\ K$, 20 K, 100 K, and 300 K collected using the GEM diffractometer at ISIS.

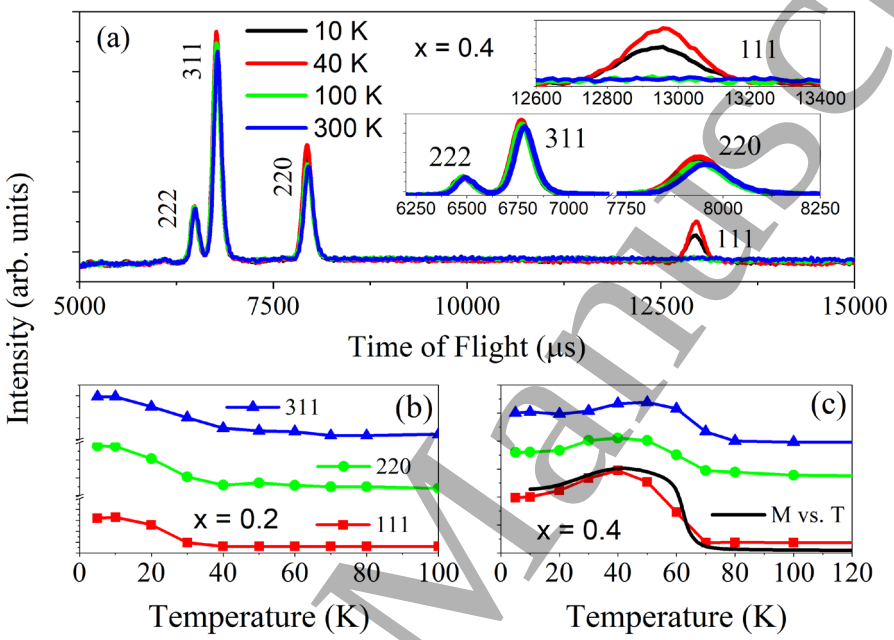

Figure 4. (a) NPD obtained at GEM (ISIS, UK) for $Tb_{0.4}Pr_{0.6}Al_2$ at $T = 10\ K$, 40 K, 100 K and 300 K. Three Bragg reflections are highlighted: (111); (220) and (311). These reflections show magnetic contributions below T_C. (b) Evolution of the amplitude of the magnetic peaks as a function of temperature for $Tb_{0.2}Pr_{0.8}Al_2$. (c) Comparison between the amplitude of the magnetic peaks and $M\ vs.\ T$ scaled curves for $Tb_{0.4}Pr_{0.6}Al_2$.

From Figure 4(b) and Figure 4(c), for $Tb_{0.2}Pr_{0.8}Al_2$ and $Tb_{0.4}Pr_{0.6}Al_2$, the 111 reflection is the most sensitive in terms of magnetic structure. For $x = 0.4$, the amplitude is larger at $T = 40\ K$ than at 10 K, following the M *versus* T behavior (black line), while for $x = 0.20$ a larger absolute magnetization is observed below 20 K. This behavior is different from the $x = 0.25$ sample [3], indicating that the samples with $x = 0.20$, 0.30, and 0.40, like the $x = 0.10$ sample studied in a previous work [3], do not exhibit magnetic frustration, which can indicate a smaller anisotropy when compared to $x = 0.25$.

3.3 Theoretical Approach and Calorimetric Measurements

Now we turn to the molecular field approach, also known as mean-field theory. The mean-field theory proposes to simplify systems with many degrees of freedom by replacing all interactions with an average or effective interaction. This reduces the many-body problem to an effective one-body problem, reducing the computational cost. For this, a self-consistent approach is used where initially the average of the values relative to these degrees of freedom is estimated. At the end, this average is calculated and compared with the value used, repeating the cycle until the value of this average converges [34]. In the early 20th century, Pierre Weiss interpreted the tendency of ferromagnetic materials to spontaneous magnetization by introducing a molecular field responsible for the ordering of elementary magnetic moments, which in turn depends on the spontaneous magnetization [35]. Hence the need for a self-consistent numerical approach.

To describe the magnetic bulk properties of the compounds studied in this paper, we assumed that the system consists of two magnetic sublattices, one for Tb and one for Pr ions, the following Hamiltonians must be diagonalized:

IOP Publishing Journal of Physics: Condensed Matter
J. Phys.: Condens. MatterJournal **XX** (XXXX) XXXXXX https://doi.org/XXXX/XXXX

$$\hat{\mathrm{H}}_{Tb} = -\lambda_{Tb}\langle J_{Tb}\rangle \hat{J}_{Tb} - \lambda_{Tb,Pr}\langle J_{Pr}\rangle \hat{J}_{Tb} + \hat{\mathrm{H}}_{Tb}^{CF} \quad (1)$$

$$\hat{\mathrm{H}}_{Pr} = -\lambda_{Pr}\langle J_{Pr}\rangle \hat{J}_{Pr} - \lambda_{Pr,Tb}\langle J_{Tb}\rangle \hat{J}_{Pr} + \hat{\mathrm{H}}_{Pr}^{CF} \quad (2)$$

In expressions (1) and (2), λ_{Pr} and λ_{Tb} represent the molecular field parameters of each sublattice, while $\lambda_{Tb,Pr}$ and $\lambda_{Pr,Tb}$ links them. For symmetry, we can consider $\lambda_{Pr,Tb} = \lambda_{Tb,Pr}$. The mean thermodynamic values of the total angular momentum operators, $\hat{J}_{Tb}$ and $\hat{J}_{Pr}$, are $\langle J_{Pr}\rangle$ and $\langle J_{Tb}\rangle$, respectively. As in the NPD analyses, we considered the $\langle 001\rangle$ direction, i.e., the z direction, as the easy axis, which is allowed by the cubic structure of $Tb_xPr_{1-x}Al_2$.

The crystal field Hamiltonians, represented by the $\hat{\mathrm{H}}_{Tb}^{CF}$ and $\hat{\mathrm{H}}_{Pr}^{CF}$ in expressions (1) and (2), are written using fourth and sixth-order terms and they are defined in the Lea–Leask–Wolf notation [36]:

$$\hat{\mathrm{H}}_{\delta}^{CF} = W_{\delta}\left(\frac{X_{\delta}}{F_4^{\delta}}(O_4^0|_{\delta} + 5O_4^4|_{\delta}) + \frac{1-|X_{\delta}|}{F_6^{\delta}}(O_6^0|_{\delta} - 21O_6^4|_{\delta})\right) \quad (3)$$

In expression (3), $\delta = Tb$ or Pr, W_{δ} represents the influence of the crystal field, X_{δ} is the ratio between the fourth and sixth terms for $O_4^0|_{\delta}$,$O_4^4|_{\delta}$, $O_6^0|_{\delta}$ and $O_6^4|_{\delta}$ Stevens operators. Finally, F_4^{δ} and F_6^{δ} are tabulated constants by Lea-Leask-Wolf [37], again, for each sublattice.

The averages of the component of the total angular momentum $\langle J_{\delta}\rangle$ of each sublattice, seen in expressions (1) and (2), are obtained using the following expression.

$$\langle J_{\delta}\rangle = \frac{\sum_i \langle i,\delta|\hat{J}_{\delta}|i,\delta\rangle e^{-E_{i,\delta}/k_BT}}{\sum_i e^{-E_{i,\delta}/k_BT}} \quad (4)$$

In expression (4), $E_{i,\delta}$ is the i^{th} eigenvalue of the i^{th} eigenstate $|i,\delta\rangle$, and k_B is the Boltzmann constant. Here, $\langle J_{\delta}\rangle$ depends on of the diagonalization of the Hamiltonians, i.e., it is a self-consistent system. The components of the magnetization related to each sublattice are calculated by $M_{\delta} = g_{\delta}\mu_B\langle J_{\delta}\rangle$. As usual, g_{δ} is the Landé factors and μ_B is the Bohr magneton.

To solve the problem, initial values of $\langle J_{Pr}\rangle$ and $\langle J_{Tb}\rangle$ are considered. These values can be assumed in terms of the magnetic angular momenta of Tb and Pr for T approaching $0\,K$, i.e., $\langle J_{Pr}\rangle = J_{Pr}(J_{Pr}+1)$ and $\langle J_{Tb}\rangle = J_{Tb}(J_{Tb}+1)$. By iterating the process, the eigenstates and eigenvalues can be obtained, and from those, other physical quantities can be simulated and the total magnetization as a function of temperature calculated by considering the contributions of the sublattices. In the case of $Tb_xPr_{1-x}Al_2$, the total magnetization is defined as $M = x\,M_{Tb} + (1-x)\,M_{Pr}$.

To obtain the magnetic entropy of each compound, the entropy of each sublattice is calculated from the eigenenergies $E_{i,\delta}$ and eigenstates $|i,\delta\rangle$, using the following expression [38,39].

$$S_{mag}^{\delta} = R\left[\ln\left(\sum_i e^{-E_{i,\delta}/k_BT}\right) + \frac{1}{k_BT}\frac{\sum_i E_{i,\delta}e^{-E_{i,\delta}/k_BT}}{\sum_i e^{-E_{i,\delta}/k_BT}}\right] \quad (5)$$

In expression (5), R is the gas constant. In the same way, the total entropy is obtained by considering the contribution of each sublattice, i.e. $S_{mag} = x\,S_{mag}^{Tb} + (1-x)\,S_{mag}^{Pr}$.

The total heat capacity, Cp, comprises a magnetic and a non-magnetic term, $Cp = C_{mag} + C_{lat}$. From S_{mag}, the magnetic heat capacity, $C_{mag} = T\left(\partial S_{mag}/\partial T\right)_H$, is calculated, while the electronic and lattice contributions of heat capacity, i.e. the non-magnetic contribution C_{lat}, can be assumed to be a linear function of the data from $LaAl_2$ to $LuAl_2$. This is detailed by the relation 103 in Ref. [38]. Using all these considerations, the total heat capacity curve as a function of temperature, $Cp(T)$, and the magnetization *versus* temperature, $M(T)$ were simulated using the MATHEMATICA software [40] enabling a careful analysis of theses parameters in the $Tb_xPr_{1-x}Al_2$ family.

To start the simulations, besides the values of $\langle J_{\delta}\rangle$ at $T = 0\,K$, it was necessary do define the values of seven parameters, λ_{Pr}, λ_{Tb}, $\lambda_{Tb,Pr}$, W_{Tb}, X_{Tb}, W_{Pr} and X_{Pr}, which were performed as follows[1]. We initially assumed values

[1] As previously shown, several physical quantities exhibit linear trends as a function of concentration x, such as magnetic transition, T_C, and lattice parameter, a, and even lattice heat capacity. In fact, some magnetic properties of rare earth ion in RAl_2 within the crystal field theory is assumed to not depend on the interaction of R with its surroundings, which can be taked as a classical electrostatic point charge potential. Considering all rare earth have valence 3^+, their atomic radii values are close to each other, and the small changes in the outer electronic configuration can be neglected, in this representation it is expected no significant changes in those properties that depend mostly on the

IOP Publishing Journal of Physics: Condensed Matter
J. Phys.: Condens. MatterJournal **XX** (XXXX) XXXXXX https://doi.org/XXXX/XXXX

consistent with a linear behavior for these parameters based on the known values for the compounds $TbAl_2$ and $PrAl_2$ [41]. From these initial values, a search algorithm was used to find the set that best produced the shape of $Cp\ vs.T$ and $M\ vs.T$. The experimental magnetization data was used to calculate the magnetic transition temperatures, and experimental $Cp(T)$ was chosen to implement this search approach.

At this point, it is worth highlighting a subtle difference between the studies developed by von Ranke et al. [20,21,28,42–44] and this work. These materials are characterized by the fact that the first neighbors of the rare earth ions are the aluminum ions with lattice parameter values showing negligible variation [41]. Based on these facts, von Ranke et al. generally assumed the values of the crystal field of the compounds at the extremes of the series, whereas here small changes in the lattice parameters induce variations in W_δ and X_δ, justifying an initial guess as a linear behavior.

Thus, we selected an initial set of parameters: $\langle J_{Pr}\rangle$, $\langle J_{Tb}\rangle$, λ_{Pr}, λ_{Tb}, $\lambda_{Tb,Pr}$, W_{Tb}, X_{Tb}, W_{Pr} and X_{Pr}. From them and assuming $T = 0.001\ K$, the Hamiltonians (1) and (2) are diagonalized. The first part of the algorithm iterates many times to converge $\langle J_\delta\rangle$ at each temperature. Then the obtained eigenvalues, $E_{i,\delta}$, and the eigenstates, $|i,\delta\rangle$, are used to calculate $\langle J_{Pr}\rangle$ and $\langle J_{Tb}\rangle$ using the expression (4). Subsequently, the new values of $\langle J_{Pr}\rangle$ and $\langle J_{Tb}\rangle$ are used to repeat this procedure until $\langle J_{Pr}\rangle$ and $\langle J_{Tb}\rangle$ converge. At this point, the temperature is increased using a step of $\Delta T = 1\ K$ up to final temperature $T = 150\ K$. This process generates the simulated $M(T)$ and $Cp(T)$, which is compared to the experimental data. This comparison is performed using a control parameter defined as $\bar{E}_{abs} = \sum_i^N |Cp_i(sim) - Cp_i(exp)|/N$, where $Cp_i(exp)$ and $Cp_i(sim)$ are the i^{th} point of experimental and simulated heat capacity, respectively, considering a total of N points (temperatures). Next, one of the parameters is varied, and the entire process repeated, allowing the smallest value of $\bar{E}_{abs}$ to indicate the best set of parameters. Finally, the algorithm calculates $\bar{E}_{abs}$ for the chosen set of mean field parameters and the crystalline field parameters.

Table 3. The mean field parameters λ_{Pr}, λ_{Tb} and $\lambda_{Tb,Pr}$, and the crystal field parameters, W_{Tb}, X_{Tb}, W_{Pr} and X_{Pr}, found in the simulations. For the concentrations $x = 0.00$ and 1.00, the obtained values are very close to that one available in literature *[41]*.

x	λ_{Pr} (meV)	λ_{Tb} (meV)	λ_{Pr-Tb} (meV)	W_{Pr} (meV)	W_{Tb} (meV)	X_{Pr}	X_{Tb}
0.00	0.540	-	-	-0.329	-	0.739	-
0.10	0.520	0.201	-0.014	-0.154	-0.095	0.635	0.130
0.20	0.392	0.236	-0.099	-0.258	-0.037	0.646	0.240
0.30	0.294	0.290	-0.137	-0.302	-0.030	0.665	0.320
0.40 (♦)	0.28	0.36	-0.115	-0.38	-0.02	0.69	0.47
0.50	0.245	0.426	-0.085	-0.416	-0.017	0.718	0.620
0.75	0.100	0.558	-0.015	-0.644	-0.008	0.757	0.850
1.00	-	0.660	-	-	-0.020	-	0.910

(♦) There are no experimental Cp data for $x = 0.40$ sample. These values, in red, were attributed considering the behavior of the parameters related to the other sample.

Table 3 displays the obtained set of parameters that better simulate the experimental $Cp\ vs.T$ and $M\ vs.T$ curves. Two examples are shown in Figure 5, comparing experimental and simulated values for the compounds $Tb_{0.2}Pr_{0.8}Al_2$ and $Tb_{0.5}Pr_{0.5}Al_2$, where small mismatches are due to the mean-field approximation, which does not take into account spin fluctuations. Overall, the results demonstrate an excellent agreement between the experimental data and the theoretical model, even if the model considers only one magnetic domain, whereas our compounds are multi-domain systems.

We start the analysis of the parameters presented in Table 3 with the compound $x = 0.10$ by comparing the set of parameters obtained here with those published in the previous work [3], where inelastic neutron scattering (INS) data revealed energy levels within the system that support the inclusion of quadrupolar interaction terms in the Hamiltonians, of the order of

chemical binding [41], as the melting point. Thus, as the mean field parameters and the crystalline field parameters depend on factors related to these quantities, it is reasonable to assume that these parameters might follow similar behaviors.

IOP Publishing Journal of Physics: Condensed Matter
J. Phys.: Condens. MatterJournal **XX** (XXXX) XXXXXX https://doi.org/XXXX/XXXX

$10^{-3}\ meV$. Some differences can be noticed: the parameters related to the sublattice formed by Pr ions differ by about 6% for λ_{Pr}, while it is just over 10% for X_{Pr}. The others, like W_{Tb}, which remained close to zero, and the inter-sublattices parameter, which stayed negative and also close to zero, did not change. However, X_{Tb} and λ_{Tb} changed significantly. We can argue that these differences can be explained by the quadrupolar interaction term added in the previous simulations.

Proceeding to the other compositions, with the exception of $x = 0.30$, it is worth noting that the $Tb_xPr_{1-x}Al_2$ pseudobinary system generally exhibit properties similar of the overall RAl_2 family of compounds [41]. As previously reported, as x approaches 0.26, the competition between sublattices increases, resulting in a compensation temperature. Thus, it is expected that concentrations around this value can present different behaviors and properties. For instance, the intensities of the magnetic peaks as a function of temperature for the $x = 0.25$ compound do not show similar behavior of $M(T)$, as happen for the other samples. This discrepancy might indicate either magnetic frustration or an EB like-effect. Finally, even if there are no experimental data available regarding the thermal capacity for $Tb_{0.4}Pr_{0.6}Al_2$ and the concentration value of Tb is far enough from $x = 0.26$, it is reasonable to assign values to the mean field and crystal field parameters related to this compound using the tendency shown by the other compounds. Thus, using the set of parameters highlighted in red in Table 3, Figure 6 displays the simulated curves of magnetization and heat capacity as a function of temperature, for the whole series, including $x = 0.40$.

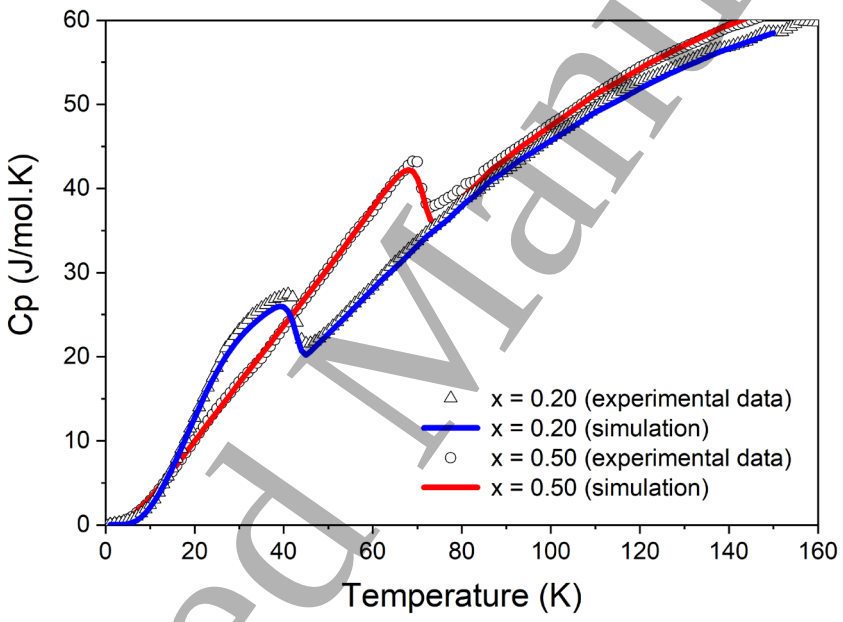

Figure 5. Comparison between experimental data (symbols) and simulated curves (lines) for $Tb_{0.2}Pr_{0.8}Al_2$ and $Tb_{0.5}Pr_{0.5}Al_2$. All other curves present similar match.

To quantify the quality of the simulations, two agreement indices were defined, $\tilde{\chi}^2$ and $\tilde{R}^2$.

$$\tilde{\chi}^2 = \frac{1}{N}\sum_{i=1}^{N}\left[\frac{Cp_i(sim) - Cp_i(exp)}{\sigma_i}\right]^2 \quad (6)$$

$$R^2 = \frac{\sum_{i=1}^{N}[Cp_i(sim) - Cp_i(exp)]^2}{\sum_{i=1}^{N}[Cp_i(exp) - \langle Cp(exp)\rangle]^2} \quad (7)$$

In Eq. (6), $\tilde{\chi}^2$ represents how well the experimental data and the used theoretical modeling match. σ_i is the experimental deviation of each Cp data. Based on the mass measurement in the heat capacity data acquirements, we assume a value of 10%, i.e., $\sigma_i = 0.1Cp_i(exp)$. Additionally, the average $\langle Cp(exp)\rangle$ is defined, $\langle Cp(exp)\rangle = (1/N)\sum_{i=1}^{N} Cp_i(exp)$. This value is used to calculate $\tilde{R}^2$ in Eq. (7). $\tilde{R}^2$ is the coefficient that can be considered a measure of adjustment of a generalized statistical model, expressing the amount of data variance compared to a linear model.

The $\tilde{\chi}^2$ and $\tilde{R}^2$ values displayed in Table 4 indicate that the simulations represent the experimental behavior of $Cp(T)$

IOP Publishing Journal of Physics: Condensed Matter
J. Phys.: Condens. MatterJournal **XX** (XXXX) XXXXXX https://doi.org/XXXX/XXXX

very well for all samples. This can be visually inspected in Figure 5 for $x = 0.20$ and 0.50 compounds. In fact, there is a great deal of agreement between theory and experiment.

Figure 7 displays the evolution of the parameters obtained by the approach described here as a function of concentration. The molecular field parameters are presented in Figure 7(a). It is important to remark that these parameters, which describe the intensity of the interactions between the ions of the sublattices, Pr–Pr (λ_{Pr}) and Tb–Tb (λ_{Tb}), have a direct influence on T_C, show a linear trend as other physical characteristics. While λ_{Pr} decreases with concentration x, λ_{Tb} increases as a compensation effect. This is expected as observed in other similar families of compounds [21,28,42,45]. The values obtained for λ_{Pr} and λ_{Tb} are positive due to the ferromagnetic coupling Tb-Tb and Pr-Pr. On the other hand, the inter-lattices parameters $\lambda_{Pr,Tb}$ are negative in the whole range of x, indicating antiferromagnetic coupling between Tb and Pr sublattices. It is interesting to note that $|\lambda_{Pr,Tb}|$ is always smaller than λ_{Tb} and λ_{Pr}, indicating that the FM coupling is larger than the AF coupling. Trend lines of $\lambda_{Pr}(x)$ and $\lambda_{Tb}(x)$ intersect around $x = 0.25$, close to 0.26, exactly at the concentration of larger competition between the sublattices. Similarly, $\lambda_{Tb,Pr}$ exhibits a minimum around this value of x. Further away from $x = 0.25$, $\lambda_{Tb,Pr}$ tends to approach zero, indicating the decreasing interactions between Pr and Tb sublattices.

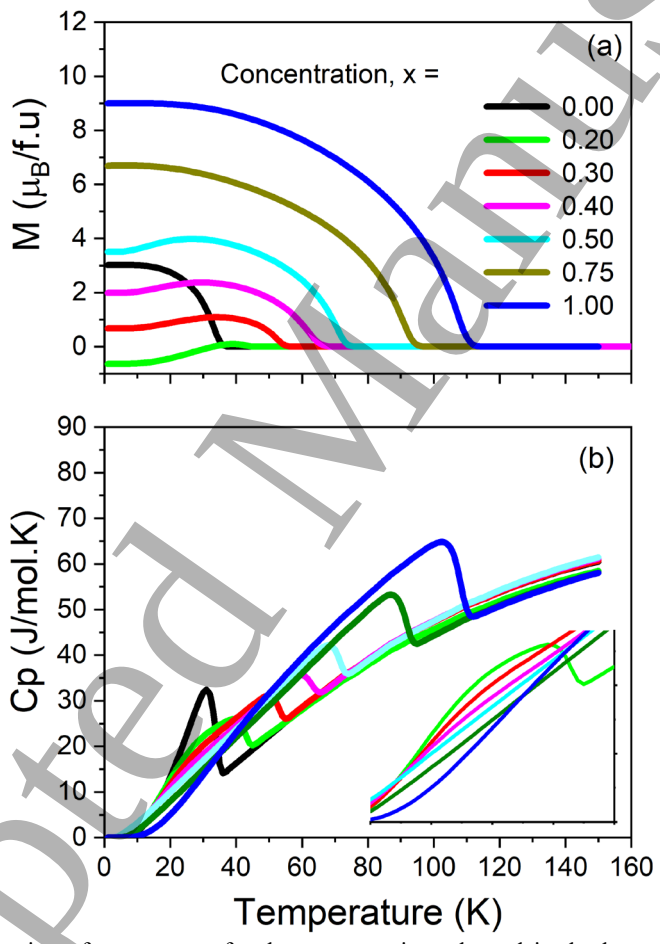

Figure 6. (a) Magnetization in function of temperature for the concentrations showed in the legend. (a) Heat capacity as function of temperature using the same color grade. In the inset are the details of the curves around $T = 30\ K$.

Figure 7 displays the evolution of the parameters obtained by the approach described here as a function of concentration. The molecular field parameters are presented in Figure 7(a). It is important to remark that these parameters, which describe the intensity of the interactions between the ions of the sublattices, Pr–Pr (λ_{Pr}) and Tb–Tb (λ_{Tb}), have a direct influence on T_C, show a linear trend as other physical characteristics. While λ_{Pr} decreases with concentration x, λ_{Tb} increases as a compensation effect. This is expected as observed in other similar families of compounds [21,28,42,45]. The values obtained for λ_{Pr} and λ_{Tb} are positive due to the ferromagnetic coupling Tb-Tb and Pr-Pr. On the other hand, the inter-lattices parameters $\lambda_{Pr,Tb}$ are negative in the whole range of x, indicating antiferromagnetic coupling between Tb and Pr sublattices.

IOP Publishing Journal of Physics: Condensed Matter
J. Phys.: Condens. MatterJournal **XX** (XXXX) XXXXXX https://doi.org/XXXX/XXXX

It is interesting to note that $|\lambda_{Pr,Tb}|$ is always smaller than λ_{Tb} and λ_{Pr}, indicating that the FM coupling is larger than the AF coupling. Trend lines of $\lambda_{Pr}(x)$ and $\lambda_{Tb}(x)$ intersect around $x = 0.25$, close to 0.26, exactly at the concentration of larger competition between the sublattices. Similarly, $\lambda_{Tb,Pr}$ exhibits a minimum around this value of x. Further away from $x = 0.25$, $\lambda_{Tb,Pr}$ tends to approach zero, indicating the decreasing interactions between Pr and Tb sublattices.

Table 4. The values of $\tilde{\chi}^2$ e $\tilde{R}^2$ for the $Tb_xPr_{1-x}Al_2$ pseudobinary system. $\tilde{R}^2$ always displays values above 99.8%, while $\tilde{\chi}^2 = 3.301$ for $x = 1.00$, all the other samples present $\tilde{\chi}^2 < 1$.

Concentration	$\tilde{\chi}^2$	$\tilde{R}^2$(%)
0.00	0.294	99.992
0.10	0.033	99.999
0.20	0.066	99.998
0.30	0.043	99.999
0.50	0.038	99.997
0.75	0.464	99.987
1.00	3.301	99.897

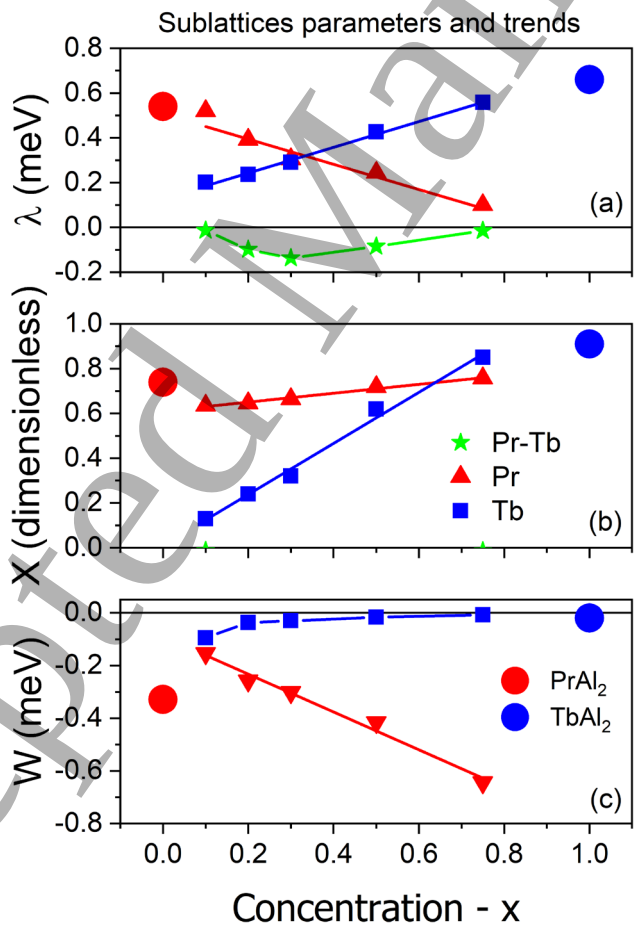

Figure 7. (a) Molecular field parameters λ_{Pr}, λ_{Tb} and $\lambda_{Tb,Pr}$ in function of x. (b) Crystal field parameters X_{Pr} and X_{Tb} *versus* concentration. (c) Crystal field energy parameters scale W_{Pr} and X_{Tb} in terms of x.

Other parameters that follow the linear trends were X_{Tb} and X_{Pr} for the rare earth mixed compounds, as shown in

IOP Publishing Journal of Physics: Condensed Matter
J. Phys.: Condens. MatterJournal **XX** (XXXX) XXXXXX https://doi.org/XXXX/XXXX

Figure 7(b). However, as it can be seen that X_δ for $TbAl_2$ and $PrAl_2$ show deviations from the linear trends observed for the other members of the family. X_{Tb} shows a very upward linear tendency, exhibiting a more expressive increase with concentration than X_{Pr}. As for other physical quantities for (R1,R2)Al_2, it is intuitively expected that these parameter values tend linearly to the extremes of the series. However, the X_{Pr} parameter shows a behavior opposite to the Tb sublattice case, as this value increases linearly and slightly as the concentration of Pr decreases. Considering that the X_{Pr} values have a much smaller variation than the X_{Tb} values, as can be seen in Figure 7(b), this contribution is almost negligible.

In the crystal field theory approach, it is assumed that neighboring ions of the rare earth ions act as point charges. Consequently, the H^δ Hamiltonians can be understood as expansions based on spherical harmonics, where X_δ represents the weighting of fourth-order terms compared to sixth-order terms in the Lea-Leask-Wolf notation [37,46]. The values of X_δ depend on the local symmetry of the site where the rare earth ion is located. In this case, there are two tetrahedral cavities of different sizes formed by equivalent sites with cubic point symmetry (T_d) that are occupied by rare earth ions. At room temperature, $PrAl_2$ has a lattice parameter approximately 2% lower than $TbAl_2$. In fact, Pr and Tb ions atomic radii values are 2.67 Å and 2.37 Å, respectively. These slight differences may be sufficient to explain small distortions at the local site, as reflected by the X_δ parameters.

Of higher interest is the evolution of the W_δ parameters that represent the influence of the crystal field intensity. In Figure 7(c) two behaviors are observed: while W_{Pr} values show a linear decrease as the concentration increases, for Tb a tendency to a threshold is observed between $x = 1.00$ and $x = 0.20$, with a small deviation for $x = 0.10$. This might indicate that Tb is less influenced than Pr by the crystalline field. In fact, in whole range of x, $|W_{Tb}| < |W_{Pr}|$, and this difference is probably connected with the orbital quantum numbers of Tb ($L_{Tb} = 3$) and Pr ($L_{Pr} = 5$). After all, the interaction with the crystalline field is directed associated to this value. This might also explain the differences in set of parameters for the $x = 0.10$ sample.

4. Comments and conclusions

In this paper, we demonstrated that the structural and magnetic properties of $Tb_xPr_{1-x}Al_2$ can be accurately simulated and interpreted by a theoretical model based on the molecular field approach. Excellent agreement between the calculated and experimental heat capacity and magnetization curves as functions of temperature was obtained by assuming two magnetic sub-lattices coupled through two Hamiltonians. By iteratively applying a developed robust search algorithm in a self-consistent system, the parameters in the model were optimized and the obtained values reproduced the experimental data. In addition, the statistical quantities and visual inspection confirmed the agreement. The obtained results described the behavior of crystal field and mean field parameters for the entire phase diagram.

Furthermore, the magnetic, calorimetric and diffraction data allowed the determination of the magnetic transition temperatures and lattice parameters, which were shown to be linear as a function of ion concentration. When describing the properties of rare earth ion in RAl_2 within the framework of the crystal field model, it is assumed that the interaction of rare earth with its surroundings can be expressed in terms of a classical electrostatic point charge potential. In this picture, it is assumed that all rare earth atoms have the same valence value and with similar atomic radii. In fact, since the outer electronic configuration does not change much, no significant changes are expected in those properties since they depend mostly on the chemical binding. This interpretation corroborates with the findings reported here

On other hand, we still observe some deviations that can be explained by our simplified theoretical model approach. One example is $X_{Pr}(x)$ which increases with Tb-concentration; the other is that although the evolution of the lattice parameter greatly affects most parameters it does not impact on W_{Tb}. This can be related to the angular *momenta*.

Author contributions

Julio C. G. Tedesco and Heloisa N. Bordallo conceived the study and wrote the manuscript. Vagner Jandre and Julio C. G. Tedesco performed the computational simulations. Alexandre Magnus G. Carvalho, Julio C. G. Tedesco and Adelino A. Coelho produced the samples. Winfried Kockelmann, Daniel M. Többens, Julio C. G. Tedesco and Heloisa N. Bordallo performed neutron powder diffraction experiments. Lisandro P. Cardoso carried out data acquisition from X-ray diffraction experiments. All authors discussed the results and worked on the manuscript.

Declaration of competing interest

The authors declare that they have no known competing financial interests or personal relationships that could have appeared to influence the work reported in this paper.

Acknowledgments

The research of Julio C. G. Tedesco at the NBI was supported by the Brazilian Science Without Borders program (funds from CNPq), and further support was also provided by the Brazilian agencies FAPESP, Capes and CNPq. The work performed at the large-scale facilities by Julio C. G. Tedesco and Heloisa N. Bordallo was financed by Danscatt, while measurements performed on E9 (Helmholtz-Zentrum Berlin) were supported by the European Commission under the 7th Framework Programme through the 'Research Infrastructures' action of the 'Capacities' Programme, NMI3-II Grant number 283883. The authors gratefully acknowledge ISIS for the provision of beam time (DOI:10.5286/ISIS.E.RB1410496). This study was financed in part by the Coordenação de Aperfeiçoamento de Pessoal de Nível Superior - Brasil (CAPES) - Finance Code 001.

References

[1] Gschneidner K A and Pecharsky V K 2008 Thirty years of near room temperature magnetic cooling: Where we are today and future prospects *Int. J. Refrig.* **31** 945–61

[2] Tishin A M, Spichkin Y I, Zverev V I and Egolf P W 2016 A review and new perspectives for the magnetocaloric effect: New materials and local heating and cooling inside the human body *Int. J. Refrig.* **68** 177–86

[3] Tedesco J C G, Carvalho A M G, Christensen N B, Kockelmann W, Telling M T F, Yokaichiya F, Többens D M, Simeoni G G, Cardoso L P, Coelho A A and Bordallo H N 2015 Analysis of the crystallographic and magnetic structures of the Tb0.1Pr0.9Al2 and Tb0.25Pr0.75Al2 magnetocaloric compounds by means of neutron scattering *J. Mater. Sci.* **50** 2884–92

[4] Shir F, Mavriplis C, Bennett L H and Torre E D 2005 Analysis of room temperature magnetic regenerative refrigeration *Int. J. Refrig.* **28** 616–27

[5] Zverev V and Tishin A M 2016 Magnetocaloric Effect: From Theory to Practice *Reference Module in Materials Science and Materials Engineering* (Elsevier)

[6] Pecharsky V K and Gschneidner Jr K A 1999 Magnetocaloric effect and magnetic refrigeration *J. Magn. Magn. Mater.* **200** 44–56

[7] A . M . Tishin and Y . I . Spichkin 2003 *The Magnetocaloric Effect and Its Applications* (UK: IoP - Institute of Physics Publishing)

[8] Tishin A M and Spichkin Y I 2014 Recent progress in magnetocaloric effect: Mechanisms and potential applications *Int. J. Refrig.* **37** 223–9

[9] Charles Geoffrey Blythe Garrett 1954 *Magnetic cooling* (New York, USA: Wiley)

[10] Lacour D, Jaffres H, Dau F N V, Petroff F, Vaures A and Humbert J 2002 Field sensing using the magnetoresistance of IrMn exchange-biased tunnel junctions *J. Appl. Phys.* **91** 4655–8

[11] Daughton J, Brown J, Chen E, Beech R, Pohm A and Kude W 1994 Magnetic field sensors using GMR multilayer *IEEE Trans. Magn.* **30** 4608–10

[12] Lenz J and Edelstein S 2006 Magnetic sensors and their applications *IEEE Sens. J.* **6** 631–49

[13] Tsang C, Fontana R E, Lin T, Heim D E, Speriosu V S, Gurney B A and Williams M L 1994 Design, fabrication and testing of spin-valve read heads for high density recording *IEEE Trans. Magn.* **30** 3801–6

[14] Tsang C 1984 Magnetics of small magnetoresistive sensors (invited) *J. Appl. Phys.* **55** 2226–31

[15] R. G. Ross Jr. 2001 *Cryocoolers* vol 11 (New York, USA: Kluwer Academic Publishers / Plenum Publishers)

IOP Publishing Journal of Physics: Condensed Matter
J. Phys.: Condens. MatterJournal **XX** (XXXX) XXXXXX https://doi.org/XXXX/XXXX

[16] Kools J C S 1996 Exchange-biased spin-valves for magnetic storage *IEEE Trans. Magn.* **32** 3165–84

[17] Julio C. G. Tedesco, Heloisa N. Bordallo, Sven Landsgesell, Alexandre Magnus Carvalho, Lisandro Cardoso, and Adelino Coelho 2014 Efficient materials for cryogenic refrigeration: The interplay of the magnetocaloric effect and electrical resistivity in TbxPr1-xAl2 ferrimagnetic compounds can help realize more efficient and advanced materials for cryogenic refrigeration *Magn. Technol. Int.* 58–61

[18] Phan T-L, Zhang P, Dan N H, Yen N H, Thanh P T, Thanh T D, Phan M H and Yu S C 2012 Coexistence of conventional and inverse magnetocaloric effects and critical behaviors in Ni50Mn(50−x)Sn(x) (x = 13 and 14) alloy ribbons *Appl. Phys. Lett.* **101** 212403

[19] Krenke T, Duman E, Acet M, Wassermann E F, Moya X, Mañosa L and Planes A 2005 Inverse magnetocaloric effect in ferromagnetic Ni–Mn–Sn alloys *Nat. Mater.* **4** 450–4

[20] Carvalho A M G, Garcia F, Sousa V S R de, von Ranke P J, Rocco D L, Loula G D, Carvalho E J de, Coelho A A, Silva L M da and Gandra F C G 2009 Magnetic coupling between Gd and Pr ions and magnetocaloric effect in Gd0.5Pr0.5Al2 compound *J. Magn. Magn. Mater.* **321** 3014–8

[21] Sousa V S R de, Carvalho A M G, Plaza E J R, Alho B P, Tedesco J C G, Coelho A A, Oliveira N A de and von Ranke P J 2011 Investigation on the magnetocaloric effect in (Gd,Pr)Al2 solid solutions *J. Magn. Magn. Mater.* **323** 794–8

[22] Tedesco J C G, Pires M J M, Carvalho A M G, de Sousa V S R, Cardoso L P and Coelho A A 2013 Exchange-bias-like effect in Pr0.75Tb0.25Al2 and Pr0.7Tb0.3Al2 samples *J. Magn. Magn. Mater.* **339** 6–10

[23] Kulkarni P D, Nigam A K, Ramakrishnan S and Grover A K 2010 *Field induced changes across magnetic compensation in Pr(1-x)Gd(x)Al(2) alloys*

[24] Kulkarni P D, Thamizhavel A, Rakhecha V C, Nigam A K, Paulose P L, Ramakrishnan S and Grover A K 2009 Magnetic compensation phenomenon and the sign reversal in the exchange bias field in a single crystal of Nd0.75Ho0.25Al2 *Europhys. Lett.* **86** 47003

[25] Williams W G, Ibberson R M, Day P and Enderby J E 1997 GEM — General materials diffractometer at ISIS *Phys. B Condens. Matter* **241–243** 234–6

[26] Többens D M, Stüßer N, Knorr K, Mayer H M and Lampert G 2001 E9: The New High-Resolution Neutron Powder Diffractometer at the Berlin Neutron Scattering Center *Mater. Sci. Forum* **378–381** 288–93

[27] Rodríguez-Carvajal J 1993 Recent advances in magnetic structure determination by neutron powder diffraction *Phys. B Condens. Matter* **192** 55–69

[28] de Sousa V S R, Plaza E J R, Reis M S, Alho B P, Carvalho A M G, Gama S, de Oliveira N A and von Ranke P J 2009 Investigation on the magnetocaloric effect in DyNi2, DyAl2 and Tb1−nGdnAl2 (n=0, 0.4, 0.6) compounds *J. Magn. Magn. Mater.* **321** 3462–5

[29] Olsen C E, Arnold G and Nereson N 1967 Magnetic Properties of PrAl2 *J. Appl. Phys.* **38** 1395–6

[30] Nereson N, Olsen C and Arnold G 1968 Magnetic Properties of PrAl2 and ErAl2 *J. Appl. Phys.* **39** 4605–9

[31] Oesterreicher Hans 1974 Constitution of aluminum base rare earth alloys RT2-RAl2 (R = Praseodymium, gadolinium, erbium; T = manganese, iron, cobalt, nickel, copper) *Inorg. Chem.* **13** 2807–11

[32] Campoy J C P, Plaza E J R, Coelho A A and Gama S 2006 Magnetoresistivity as a probe to the field-induced change of magnetic entropy in RAl2 compounds (R=Pr,Nd,Tb,Dy,Ho,Er) *Phys. Rev. B* **74** 134410

[33] Kulkarni P D, Venkatesh S, Thamizhavel A, Rakhecha V C, Ramakrishnan S and Grover A K 2009 Exchange Bias and Its Phase Reversal in Zero Magnetization Admixed Rare-Earth Intermetallics *IEEE Trans. Magn.* **45** 2902–6

[34] Chaikin P M and Lubensky T C 2000 *Principles of Condensed Matter Physics* (Cambridge: Cambridge University Press)

[35] Magnani N 2005 Ferromagnetism *Encyclopedia of Condensed Matter Physics* ed F Bassani, G L Liedl and P Wyder (Oxford: Elsevier) pp 201–10

IOP Publishing Journal of Physics: Condensed Matter
J. Phys.: Condens. MatterJournal **XX** (XXXX) XXXXXX https://doi.org/XXXX/XXXX

[36] Jens Jensen and Allan R. Mackintosh 1991 *Rare earth magnetism : structures and excitations* (Oxford: Oxford University Press)

[37] Lea K R, Leask M J M and Wolf W P 1962 The raising of angular momentum degeneracy of f-Electron terms by cubic crystal fields *J. Phys. Chem. Solids* **23** 1381–405

[38] Oliveira N A de and Ranke P J von 2010 Theoretical aspects of the magnetocaloric effect *Phys. Rep.* **489** 89–159

[39] Smart J S 1966 *Effective field theories of magnetism* (Saunders)

[40] Wolfram Research Inc 2022 Mathematica

[41] Purwins H G and Leson A 1990 Magnetic properties of (rare earth)Al2 intermetallic compounds *Adv. Phys.* **39** 309–403

[42] Alho B P, Ribeiro P O, Alvarenga T S T, Carvalho A M G and Von Ranke P J 2014 Magnetocaloric effect in Gd(1−y)DyyAl2 *Int. J. Refrig.* **37** 297–302

[43] Lima A L, Oliveira I S, Gomes A M and von Ranke P J 2002 Origin of anomalous magnetocaloric effect in (Dy_{1-z}Er_{z})Al_{2} alloys *Phys. Rev. B* **65** 172411

[44] Ribeiro P O, Alho B P, Alvarenga T S T, Nóbrega E P, de Sousa V S R, Carvalho A M G, Caldas A, de Oliveira N A and von Ranke P J 2015 Theoretical investigations on magnetocaloric effect in Er1−yTbyAl2 series *J. Magn. Magn. Mater.* **379** 112–6

[45] Alho B P, Lopes P H O, Ribeiro P O, Alvarenga T S T, Nóbrega E P, de Sousa V S R, Carvalho A M G, Caldas A, Tedesco J C G, Coelho A A, de Oliveira N A and von Ranke P J 2018 Magnetic and magnetocaloric properties in Gd1−yPryNi2 compounds *J. Magn. Magn. Mater.* **449** 308–12

[46] M.T. Hutchings 1964 Point-Charge Calculations of Energy Levels of Magnetic Ions in Crystalline Electric Fields *Solid State Physics* vol Volume 16 (Academic Press) pp 227–73